# cmgh

ORIGINAL RESEARCH

Longitudinal Single-Cell Transcriptomics Reveals a Role for Serpina3n-Mediated Resolution of Inflammation in a Mouse Colitis Model

Yen-Ting Ho,[1] Takashi Shimbo,[1] Edward Wijaya,[1,2] Tomomi Kitayama,[1,2] Satoshi Takaki,[1] Kentaro Ikegami,[2] Kazuya Miyashita,[2] Yuya Ouchi,[1,2] Eiichi Takaki,[1,2] Ryoma Yamamoto,[1,2] Yasufumi Kaneda,[3] and Katsuto Tamai[1]

[1]Department of Stem Cell Therapy Science, Graduate School of Medicine, Osaka University, Suita, Japan; [2]StemRIM Inc, Ibaraki, Osaka, Japan; and [3]Division of Gene Therapy Science, Graduate School of Medicine, Osaka University, Suita, Japan
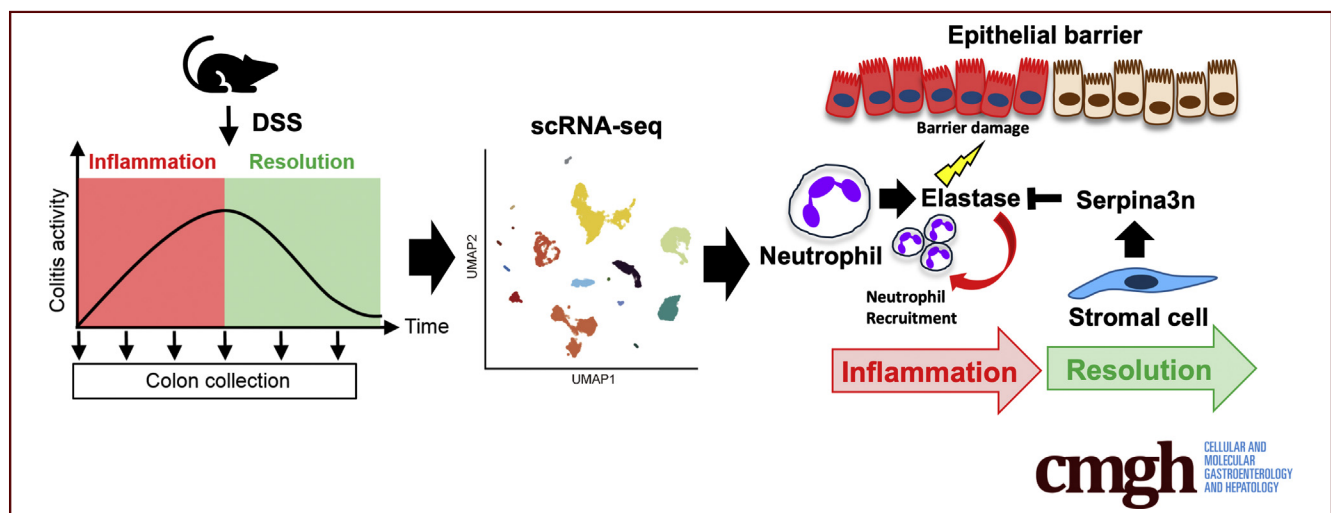
SUMMARY

This study dissected the dynamic changes during inflammation using single-cell RNA-seq. We identified that Serpina3n, expressed in the damaged stromal cells, has critical roles in the resolution of inflammation. Our data will serve as a foundation to understand inflammatory diseases.

BACKGROUND & AIMS: Proper resolution of inflammation is essential to maintaining homeostasis, which is important as a dysregulated inflammatory response has adverse consequences, even being regarded as a hallmark of cancer. However, our picture of dynamic changes during inflammation remains far from comprehensive.

METHODS: Here we used single-cell transcriptomics to elucidate changes in distinct cell types and their interactions in a mouse model of chemically induced colitis.

RESULTS: Our analysis highlights the stromal cell population of the colon functions as a hub with dynamically changing roles over time. Importantly, we found that Serpina3n, a serine protease inhibitor, is specifically expressed in stromal cell clusters as inflammation resolves, interacting with a potential target, elastase. Indeed, genetic ablation of the *Serpina3n* gene delays resolution of induced inflammation. Furthermore, systemic Serpina3n administration promoted the resolution of inflammation, ameliorating colitis symptoms.

CONCLUSIONS: This study provides a comprehensive, single-cell understanding of cell-cell interactions during colorectal inflammation and reveals a potential therapeutic target that leverages inflammation resolution. *(Cell Mol Gastroenterol Hepatol 2021;12:547–566; https://doi.org/10.1016/j.jcmgh. 2021.04.004)*

Keywords: Serpina3n; Colitis; Stromal Cell; Single Cell RNA-Sequencing.

Inflammation is a complex and highly coordinated biological event whose dysregulation is linked to a variety of diseases including cancer.[1] Upon tissue damage, neutrophils are quickly recruited. Subsequent crosstalk between resident and mobilized cells in the affected tissue can initiate and amplify an inflammatory response. Ordinarily these mobilized neutrophils are then removed by macrophages, thus resolving inflammation. This sequence in the inflammatory response is essential for the removal of the initial

trigger. However, excessive or prolonged accumulation of neutrophils can lead to chronic inflammation resulting in tissue and organ damage.[2] Thus, the inflammatory response must be tightly regulated to maintain homeostasis.

Inflammatory bowel diseases (IBDs), which include ulcerative colitis and Crohn's disease, are chronic inflammatory disorders with unknown etiology.[3] Chronic inflammation and colitis are observed in the colon (ulcerative colitis) or gastrointestinal tract (Crohn's disease); IBD patients suffer from severe diarrhea and stomach pain.[4] IBD is characterized by the loss of intestinal epithelial integrity.[5] Upon tissue damage, the microbiota and their associated products trigger the inflammatory cascade.[6] Dendritic cells recognize infiltrating antigens and ignite inflammation by activating multiple immune cell types, including macrophages, neutrophils, and T cells. Prolonged activation of this inflammatory cascade damages the intestinal epithelium and stromal cells, leading to an inability to maintain homeostasis. In contrast to healthy individuals, inflammatory resolution is not properly induced in IBD patients, and acute inflammation often shifts to chronic inflammation. Although recently introduced therapeutics such as anti–tumor necrosis factor antibodies show promise for treating IBD, roughly half of the patients are still refractory to available treatment options.[7] In addition, it is well-known that flares, sudden acute inflammation, occur even in patients with symptoms under control.[8] It is therefore essential to understand the detailed mechanisms of how inflammation is initiated and resolved in IBD to establish more broadly effective approaches to controlling disease. However, a comprehensive molecular and cellular map that includes the complex and dynamic cascades linked to inflammation is currently unavailable.

To gain a comprehensive and dynamic view of the inflammatory process, we analyzed cells over time in an unbiased manner, in contrast to previous studies that focused on specific cell types such as macrophages or epithelial cells.[9] This allowed us to dissect complex changes linked to inflammations in a biological context. We analyzed the initiation and disappearance of inflammation at the single-cell level using a mouse model of colitis. Single-cell transcriptomics was used to describe the dynamic molecular and cellular responses during inflammation. As a result, we identified and validated an important role for the serine protease inhibitor clade A member 3N (Serpina3n) during inflammation and suggest that it provides a therapeutic avenue for interfering with the adverse effects of an uncontrolled inflammatory response.

Results

Single Cell RNA-Sequencing Analysis on a Mouse Colitis Model

Comprehensive molecular and cellular characterization during the course of inflammation requires a well-regulated model that allows dissection of different stages of inflammation. To model human IBD over time, we chose a well-established mouse colitis model that is induced by dextran sulfate sodium (DSS).[10] We treated mice with 1.5% DSS in drinking water for the first 6 days and then switched to regular drinking water. The decrease in body weight, related to colon inflammation, reached a low point at day 9 and then gradually recovered (Figure 1A). Histologic assessment also showed gradual progression and resolution of inflammation in this DSS-induced mouse colitis model (Figure 1B and C). To perform single-cell RNA sequencing (RNA-seq), we sequentially collected colon samples after DSS-mediated induction (days 0, 3, 6, 9, 12, and 15). We prepared 3 biological replicates for each time point and combined these to reduce mouse-to-mouse variability. We analyzed all viable cells in the colon using a fluorescence-activated cell sorting–based Smart-Seq2 method.[11] We profiled 14,624 cells in total from 18 mice at 6 different time points. We first combined all data and identified 15 cell clusters that were based on the gene expression profiles (Figure 1D). We annotated cell types using SingleR[12] and previously described cell-specific markers (Figure 1E, Figure 2A).[13–17] The 15 cell clusters included a cluster representing mononuclear phagocytes (MNPs) (C1) expressing *Il1b, C1qa,* and *C1qb.* Two epithelial cell clusters were present in our analysis: enteroendocrine cells (epithelial: enteroendocrine cells) (C2) expressing *Scgn* and *Pcsk1n,* and absorptive and secretory cells (epithelial: Abs and sec cells) (C8) expressing *Muc2, Spink4, Lypd8,* and *Elf3.* A part of these epithelial cells expressed sox9, muc4, smoc2, and ascl2, indicating the existence of epithelial stem/progenitor cells (Figure 2B).[18] We also identified an endothelial cell cluster (C3) expressing *Pecam1* and *Flt1* and a lymphatic cell cluster (C4) expressing *Lyve1.* C5 is a stromal cell cluster expressing *Col1a1, Pdgfra,* and *Spon2.* Two myofibroblast cell clusters (C6, C7) expressing *Acta2* and *Myh11* were present. We also identified a cluster containing interstitial cells of Cajal (C12) expressing *Ano1* and *Kit.* An enteric glial cell cluster (C14) expressed *S100b.* The T-cell cluster (C13) expressed *Cd3d* and *Cd3g.* C11 was a plasma cell cluster expressing *Igha* and *Mzb1.* A plasmacytoid dendritic cell cluster (C9) was defined by expression of *Siglech* and *Ccr9,* whereas the B-cell cluster (C15) expressed *Cd19* and *Cd22.* A granulocyte cluster (C10) expressed *Cd14, S100a8,* and *S100a9.* To visualize cell compositions changes in the colon during inflammation, we counted the number of the cells in each cluster at each time point (Figure 1F, Figure 2C). Likely reflecting tissue damage, the epithelial (C2 and C8), stromal, myofibroblast (C5, C6, and C7), interstitial cells of Cajal (C12), and enteric glial cell (C14) populations gradually decreased on inflammation induction. These clusters did not repopulate even during and after resolution. Anti-correlated with these changes, the

number of cells in the granulocyte (C10) and B-cell (C15) clusters significantly increased on induction of inflammation and did not come back to the steady state. The number of cells in the MNP cluster increased, peaking at day 6, and then fell back to the steady state. Interestingly, plasma cells, maintaining gut immunity by secreting immunoglobulin A, decreased most at the most severe time points (days 6 and 9) but recovered toward the resolution phase. Together, these data demonstrate that cell types in the colon dynamically shift over the course of inflammation.

Phenotypic Changes During the Course of DSS-Induced Inflammation

Next we examined phenotypic changes in each cell type during inflammation. We first evaluated the inflammation status of MNPs by calculating the inflammation score. Inflammation in MNPs peaked at day 6 and was suppressed approaching the resolution phase, suggesting that our single-cell RNA-seq data successfully capture the expected activation and resolution of MNPs during inflammation (Figure 3A). To visualize the phenotypic changes in other cell clusters, we performed a pseudotime analysis (Figure 3B). Phenotypic changes inferred by pseudotime analysis were most significant in MNPs, T cells, and stromal cells, whereas the lymphatic and plasmacytoid DC clusters were relatively stable (Figure 3C). Differentially expressed gene (DEG) analysis also showed enrichment of phenotypic changes across time points in MNPs and stromal cell clusters (Figure 3D). To clarify how these phenotypic changes correlate with colon colitis, we sought to evaluate the expressions of genes that are associated with IBD pathogenesis. On the basis of previous studies, we selected 96 genes that are implicated as "IBD risk genes"[19–24] (Table 1, Supplementary Tables 1-12). Of those 96 IBD risk genes, 79 genes were expressed at one or more time points in at least one of the cell types (Figure 4A). To further investigate expression of IBD risk genes, we focused on 60 IBD risk genes with high expression levels (Figure 4B). Of those, 19 genes (31.1%) were expressed only in one cell type, whereas 41 genes (68.3%) were expressed in multiple cell types (Figure 4C). In addition, we also found that the expression of IBD risk genes was dynamically regulated during inflammation. Together our data support dynamic and pleiotropic roles for the IBD risk genes during inflammation (Figure 4D). For example, Ifng was broadly expressed during inflammation in the T-cell cluster, whereas its expression peaked at day 6 in the stromal cell cluster. The expression of Ahr peaked at different time points when compared across different cell types (Figure 4E). These data indicate that phenotypic changes in each cell are highly dynamic, and our single-cell RNA-seq approach faithfully captures dynamic gene regulation during inflammation.

Stromal Cells Act as a Hub During Colon Inflammation

To delineate how these dynamically changing cell types interact with each other, we mapped cell-cell communication by focusing on ligands and receptors usages using NicheNet.[25] NicheNet identifies the cells expressing corresponding receptors for a particular ligand using a prior knowledge model. Counting the number of active ligands and receptors allowed us to visualize complex and dynamic interactions among various cell types during inflammation (Figure 5A, Figure 6). After removing the interactions observed before induction (day 0), we visualized the number of ligand and receptor pairs (Figure 5B). Of these interactions, we found that stromal cell clusters had the highest influence on other clusters, suggesting that they function as a hub for cell-cell interactions during inflammation (Figure 5C).

### Serpina3n Expression in the Remission Phase of DSS-Induced Inflammation

Because cell-cell interaction analysis suggested a pivotal role for stromal cells during inflammation, we next performed DEG analysis on the stromal cell cluster across different inflammatory stages. We identified 257 DEGs in stromal cells during inflammation and found that DEGs can be categorized into 4 different expression patterns (Figure 7A). The genes in patterns 1, 2, and 3 were, in general, up-regulated during early phases after induction of inflammation and down-regulated toward the resolution phase. Genes in pattern 3 showed strong up-regulation at day 3. Interestingly, we also uncovered pattern 4, in which genes were up-regulated during the resolution phase of inflammation. Among these genes, Serpina3n, a serine protease inhibitor, showed the highest expression level (Figure 7B). Serpina3n expression was most prominent during the resolution phase of inflammation and was observed almost exclusively in the stromal cell cluster (Figure 7C–F). Immunostaining and Western blot analyses also confirmed the Serpina3n expression in stromal cells in the colon (Figure 7G and H). Because Serpina3n is known to covalently bind to and inhibit serine proteases, we performed immunoprecipitation–Western blotting analysis using inflamed colon samples and identified a complex containing Serpina3n (Figure 7I). We found that elastase, a serine protease that is released during inflammation, was bound by Serpina3n, suggesting that Serpina3n inhibits the activity of at least elastase (Figure 7J). To further confirm a physiological role for Serpina3n during inflammation, we examined DSS-induced colitis using the Serpina3n knockout (Serpina3n KO) mouse (Figure 8A). Interestingly, although wild-type and Serpina3n KO mice showed a similar level of body weight decrease on DSS treatment, recovery of body weight at later time points (days 9, 12, 15) in Serpina3n KO mice was significantly reduced compared with that of wild-type mice (Figure 8B–D). These data suggest that Serpina3n is specifically induced during resolution of the DSS-induced inflammation, and this protease inhibitor functions as an endogenous regulator of the resolution phase of inflammation.

Therapeutic Potential of Serpina3n for IBD

We hypothesized that genes, or at least a subset of them, that are specifically up-regulated during the resolution

phase of inflammation can function as endogenous immunomodulators or tissue regeneration factors. If so, supplementing these specific proteins may suppress or prevent the progression of inflammation. To test this, we systemically injected purified Serpina3n into the mouse colitis model. Six shots of Serpina3n (20 μg/kg) clearly prevented
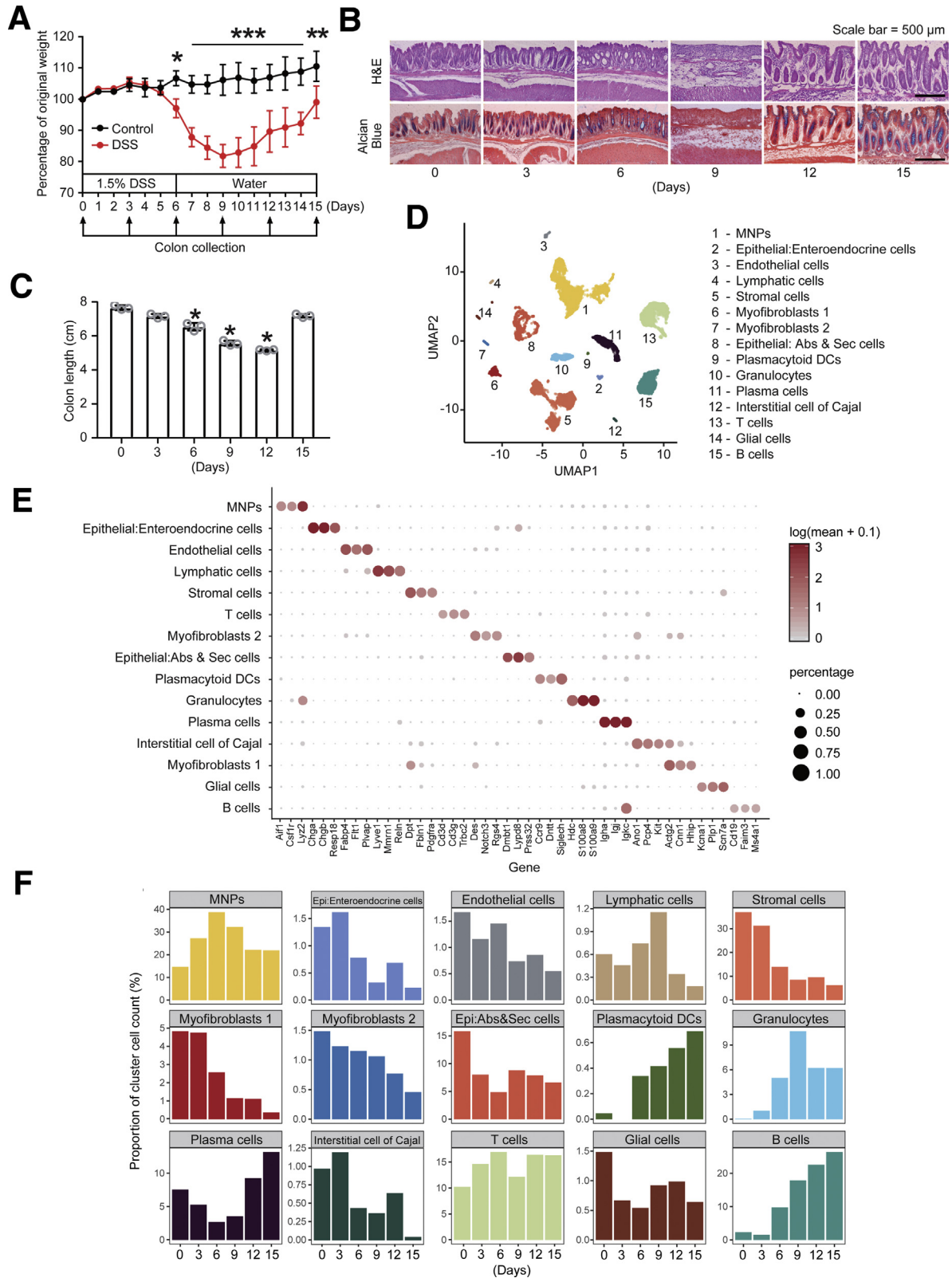
DSS-induced body weight loss (Figure 9A). Histologic evaluation of the colon supported the therapeutic impact of Serpina3n in the mouse colitis model (Figure 9B and C). To explore the mechanism by which Serpina3n treatment ameliorates DSS-induced symptoms, we performed single-cell RNA-seq analysis on the Serpina3n treated colon, along with control phosphate-buffered saline (PBS) treated colon, at day 6 (Figure 9D). Interestingly, the inflammation-induced increase in granulocyte and B-cell clusters was mitigated in the Serpina3n treated group, suggesting that Serpina3n treatment prevented the progression of inflammation (Figure 9E and F). DEG analysis indicated that expression changes upon the Serpina3n treatment were enriched in MNPs and stromal cells (Figure 9G). Evaluation of the inflammation score in MNPs also showed that inflammation became milder upon Serpina3n treatment (Figure 9H). Gene ontology analysis of DEGs in stromal cells showed enrichment in the categories of "cytokine-mediated signaling" and "extracellular matrix organization" pathways (Figure 9I). In addition, we noticed that the number of S100a8/9 positive granulocytes (likely neutrophils) was significantly reduced upon the Serpina3n treatment (Figure 9J). Furthermore, cell-cell interactions inferred by ligand-receptor analysis showed decreased interactions in the Serpina3n treated colon, presumably because inflammatory interactions were suppressed (Figure 10). Collectively, these data suggest that Serpina3n, specifically up-regulated during resolution of inflammation, can prevent the progression of inflammation.

Discussion

Inflammation involves a tightly regulated sequence of events in which various cell types dynamically change their properties and interact with each other.[26] In this study, we build a molecular and cellular atlas that follows the progression of inflammation at a single-cell level. We reveal that each cell dynamically changes in both molecular makeup and appearance in the inflamed colon. We also find that stromal cells function as a hub in this dynamic inflammatory cascade by secreting various ligands. We clarified that Serpina3n is specifically up-regulated in stromal cells during the resolution phase of inflammation. In addition, we showed that systemic injection of Serpina3n could mitigate symptoms related to IBD, presumably by moving the resolution phase of inflammation forward.

The progression and resolution of uncontrolled inflammation, and other disease, are a complex biological sequence, and each stage needs to be analyzed in detail to fully clarify molecular mechanisms. In this study, we combined a mouse colitis model with single-cell RNA-seq analysis to dissect the progression and resolution of inflammation at the single-cell level. The use of the mouse colitis model allowed us to precisely control the progression of inflammation. Although many single-cell analyses using samples of human colitis patients have been reported,[13–17] it is difficult to align each patient on the basis of the stages of the diseases. These studies missed the importance of SerpinA3, a human homolog of Serpina3n, because of the lack of enough number of patients in the resolution phase. Recently, another group reported the expression of SerpinA3/Serpina3n in the colon epithelium during IBD-type colon inflammation.[27] However, our single-cell transcriptome analysis indicated specific expression of Serpina3n in stromal cells rather than in the colon epithelium; further studies need to be conducted to the cell source of Serpina3n. In addition, our temporal single-cell RNA-seq analysis revealed that Serpina3n was up-regulated in the resolution phase during inflammation rather than in the induction phase of inflammation, which was further validated by Western blotting, immunostaining, and quantitative polymerase chain reaction (qPCR) experiments. Thus, combining studies of mouse models with temporal single-cell analysis can provide a powerful combination to understand disease progression.

We found that Serpina3n was specifically up-regulated during the resolution of inflammation in stromal cells. The Serpina3n KO mouse model failed to evoke proper resolution, indicating that Serpina3n has a physiological function in resolving inflammation. We also showed that the systemic delivery of Serpina3n could ameliorate symptoms in a mouse colitis model. Serpina3n is an endogenously coded serine protease inhibitor.[28] By covalently binding to serine proteases, such as elastase or trypsin, through its reactive center loop, Serpin family proteins irreversibly inhibit their target proteins.[29] We showed that Serpina3n is directly bound to elastase in the inflamed colon. Interestingly, we found that the number of S100a8/9 positive granulocytes (neutrophils), which is activated by elastase and known to exacerbate the inflammation, was reduced upon the Serpina3n treatment.[30,31] This suppression of the S100a8/9 positive granulocytes can be a part of the mechanisms of how Serpina3n ameliorates the disease. Although we speculate that systemically injected Serpina3n binds and inhibits proteases released from the inflamed colon, further studies will reveal the exact mechanisms involved. In addition, detailed analyses on the interactions between stromal cells and other cells such as epithelial cells, which include stem/progenitor cells and play pivotal roles in inflammation, need to be performed. Taken together, further mechanistic studies examining the endogenous roles of Serpina3n in inflammation and the

---

Figure 1. (*See previous page*). **Single-cell RNA-seq time course of induced colon inflammation.** (*A*) Scheme illustrating our time-course analysis in the murine DSS-induced colitis model. Body weight was recorded every day. Mean ± standard error of the mean is indicated. *P* values were calculated with two-way analysis of variance (ANOVA) (n = 3 mice per group). *P < .05, **P < .01, ***P < .001. (*B and C*) Colonic length was measured at each time point (days 0, 3, 6, 9, 12, and 15). *P* values were calculated with one-way ANOVA (n = 3 mice per group). *P < .05 (*B*). Histologic assessment of colon samples (days 0, 3, 6, 9, 12, and 15). The representative section was stained with H&E or alcian blue. Scale bar: 500 μm (*C*). (*D*) Data visualization using a UMAP plot. Annotated cell types are listed. (*E*) Marker genes for each cluster are illustrated. *Dot size* represents percentage of cells expressing the particular gene within the cluster. Intensity of *dot color* shows mean expression level. (*F*) Percentage of cell proportion in each cluster over time.
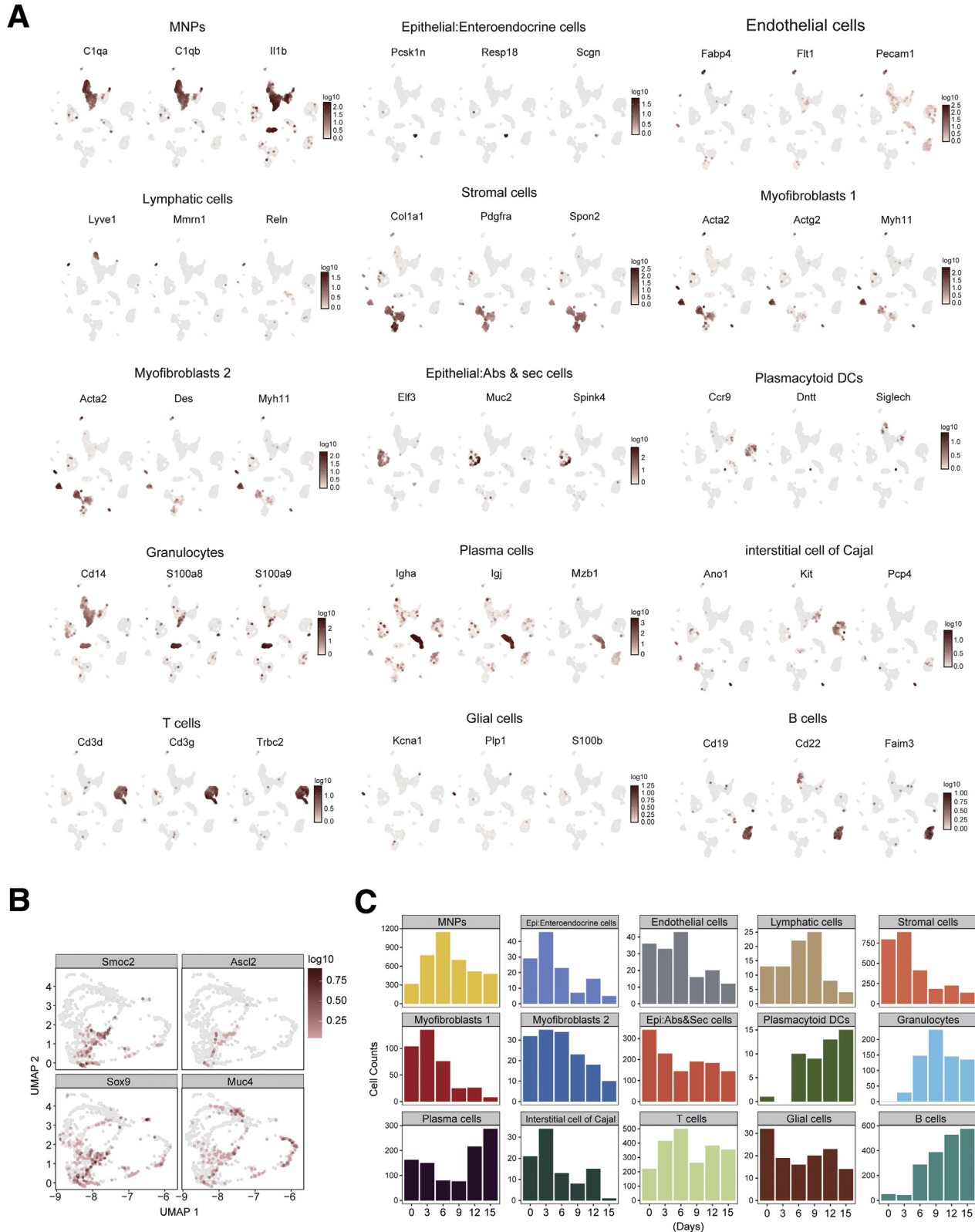
Figure 2. Marker genes of cell clusters. (*A*) Marker genes expressed on cell clusters were illustrated in the UMAP plot. (*B*) UMAP plot showing the stem/progenitor marker genes within epithelial: Abs & sec cell cluster. (*C*) Cell proportions in clusters are shown in the bar graph; *y*-axis: cell count, bottom: time point.
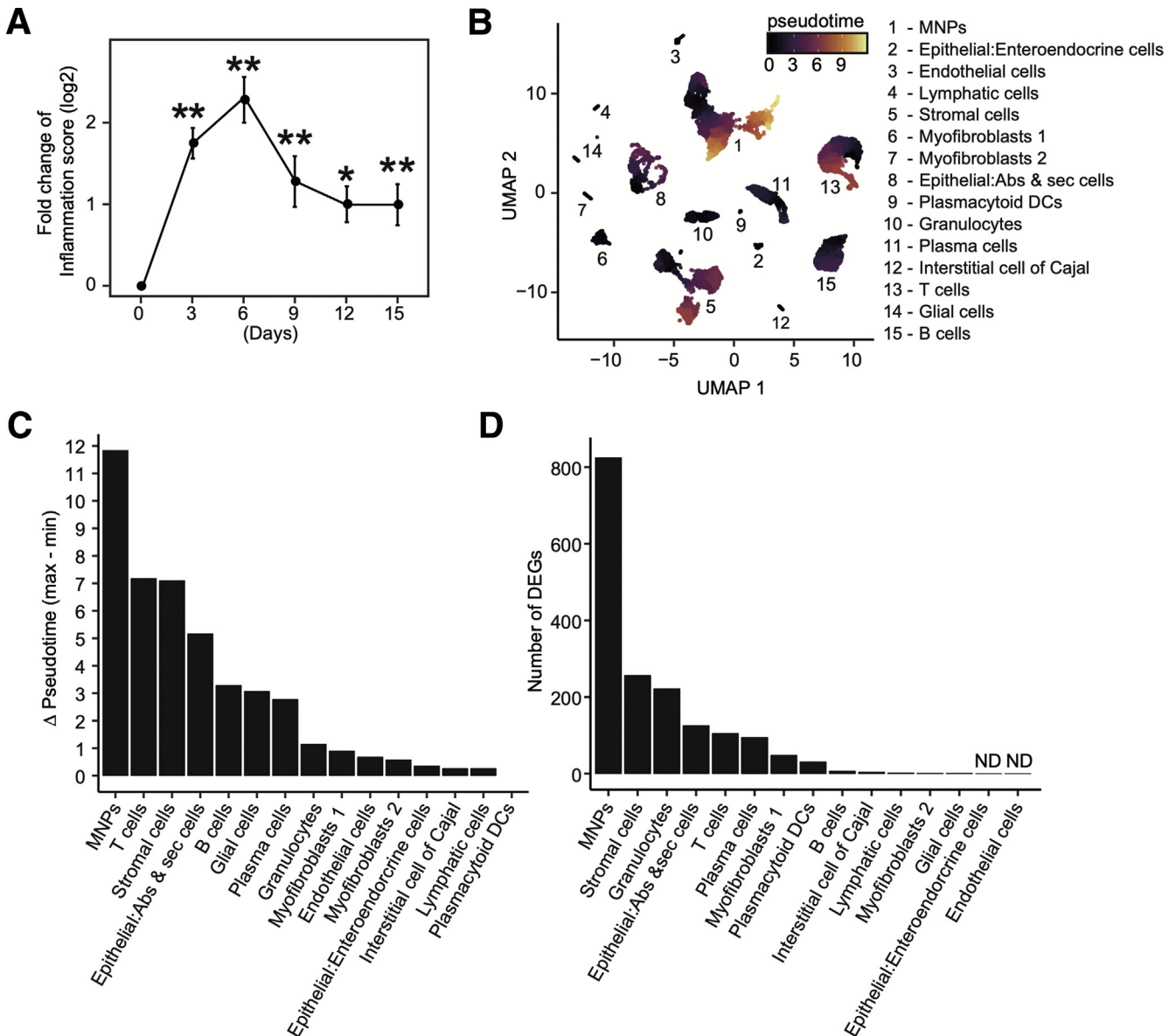
Figure 3. Phenotypic changes during inflammation. (*A*) Inflammation score was calculated on the basis of expression levels of inflammatory genes expressing in the MNP cluster. *P* values were calculated using one-way ANOVA Bonferroni post-test. *P < .01, **P < .001. (*B*) Analysis of pseudotime changes in cell clusters. (*C*) Difference between maximum and minimum pseudotime within cell clusters. (*D*) Number of DEGs in each cluster is indicated. ND, no detection of DEGs.

mechanisms underlying mitigation of inflammation need to be conducted to prepare the way for potential clinical trials.

Despite recent progress in the development of IBD therapeutics, a significant number of patients (30%–50%) remain refractory to the available treatment options.[32] To accelerate drug development for IBD, it is essential to investigate disease mechanisms deeply and leverage new techniques. Here we have combined a single-cell technique, mouse models, and gene editing to analyze dynamic changes during disease progression and remission, providing an atlas of the changing landscape in different cell types as inflammation progresses and a potential therapeutic avenue for resolving the uncontrolled inflammatory state.

Methods
Mice

C57BL/6J mice were purchased from CLEA Japan (Tokyo). All mice were housed under a 12-hour light-dark cycle and were provided solid food and filtered water. *Serpina3n* knockout mice were established with the i-GONAD[33] method using a crRNA (CAGACTTGAACGTGT-CAAGA) targeting exon3 of *Serpina3n,* designed using CHOPCHOP.[34] Mice with deletions that abrogated *Serpina3n* expression were used for this study. All animals were handled and protocols were approved by the Animal Committee of the Osaka University Graduate School of Medicine.

Table 1. IBD Risk Genes	
IBD risk genes	References
Atg16l1, Bach2, Cd40, Cd6, Ctif, Erap2, Fcgr2a, Fos, Fut2, Gpr65, Ifng, Il10, Il2ra, Il6st, Irf5, Irf8, Itln1, Jazf1, Lacc1, Mefv, Mst1, Nos2, Nrip1, Nxpe1, Prkcb, Ptger4, Ptpn22, Rasgrp1, Ripk2, Spred2, Stat4, Tmem135, Tmem258, Tnfaip3, Tnfsf15, Traf3ip2Znf831	Jostins L et al[19]
Card9, Hnf4a, Ifih1, Ikzf1, Il12b, Il23r, Inpp5e, Jak2, Nkx2-3, Prdm1, Rtel1-Tnfrsf6b, Smad3, Tyk2	Huang H et al[22]
Ahr, Auh, Btbd8, Ccl20, Cd28, Gpr32, Gpr35, Hgfac, Lrrk2, Nod2, Osmr, Ptprc, Sh2b3	Liu JZ et al[20]
Abi1, Adcy7, C11orf30, C1orf106, C5orf66, C7orf33, C7orf72, Cdkal1, Efna1, Ergic1, F5, Gckr, Gsdmb, Hla, Id4, Ifh1, Itga4, Itgav, Keap1, Ncf4, Nr5a2, Nr5aa, Osgin2, Plcg2, Rft1, Rnf186, Rorc, Rspo3. Skap2, Slc22a23, Slc39a11, Slc39a8, Tab2	de Lange KM et al[21]

DSS-Induced Mouse Colitis Model

DSS (36-50 kDa; MP Biomedicals, Santa Ana, CA) was prepared in water and filtered with a 0.45-μm cellulose acetate filter.[35] To induce colitis, 8-week-old male mice were administered with 1.5% DSS daily from days 0 to 6. At day 6, DSS treatment was stopped, and animals were switched to water until the end of experiment. To obtain a time course, colons were collected on days 0, 3, 6, 9, 12, and 15 to analyze histology and colon length. For the prophylactic trial, PBS, or recombinant murine SerpinA3N (R&D Systems, Minneapolis, MN) was intravenously injected into mice daily on days 0–5 (20 μg/kg per shot). Histology and colon length were analyzed on day 9.

Single-Cell RNA-seq

For isolation of colon cells, proximal, distal colon, and rectum were collected from each time point. We pooled 3 biological replicates in each group. Intestines were opened longitudinally and washed to remove fecal content with cold PBS, minced into small pieces, and incubated with RPMI 1640 containing 5% fetal bovine serum, 300 μg/mL Liberase TM (Roche, Basel, Switzerland), 10 U/mL DNase I (Takara Bio Inc, Shiga, Japan) for 1 hour at 37°C in a water bath. After digestion, cells were filtered through a 70-μm cell strainer, washed in RPMI 1640 with 5% fetal bovine serum, and spun down at 300g for 5 minutes to obtain a cell suspension. Single-cell RNA-seq was performed on the basis of a previous report with modifications as follows.[11] Primer mix (5 μL of lysis buffer [3.1375 μL of Buffer EB] [Qiagen, Hilden, Germany], 0.5 μL of 10 mmol/L dNTP [GenScript, Piscataway, NJ], 0.05 μL of Phusion HF buffer [New England BioLabs, Beverly, MA], 0.3125 μL of Proteinase K [Nacalai Tesque, Kyoto, Japan], and 1 μL of 1 μmol/L barcoded oligo-dT primer [5'-ACGACGCTCTTCCGATCT[Barcode]NNNNNNNN TTTTTTTTTTTTTTTTTTTTTTTTTTTTTTVN-3', where "N" is any base and "V" is "A", "C", or "G"; IDT]) was aliquoted into 384-well plates. Live cells were sorted into the plate using a BD FACSAria III instrument (BD Biosciences, San Jose, CA; 100 μm chip) using the single-cell purity mode. The plates were immediately centrifuged and frozen at –80°C. Plates were incubated at 50°C for 10 minutes and then at 80°C for 10 minutes. Five microliters of first-strand reaction mix containing 2 μL of 5× Superscript

IV First-Strand Buffer (Thermo Fisher Scientific, Waltham, MA), 0.5 μL of 100 mmol/L DTT (Thermo Fisher Scientific), 0.025 μL of SuperScript IV reverse transcriptase (200 U/μL; Thermo Fisher Scientific), 0.1 μL of SUPERase In RNase Inhibitor (Thermo Fisher Scientific), and 2.375 μL of water was aliquoted into each well. The plates were then incubated at 55°C for 10 minutes, and the reaction was inactivated by incubation at 80°C for 10 minutes. To remove unincorporated oligos, 2 μL of Exonuclease I mix containing 0.25 μL of Exonuclease I (Thermo Scientific), 1.2 μL of 10× Reaction Buffer, and 0.55 μL of water was added, and the mixture was incubated at 37°C for 20 minutes. Samples were pooled and purified using DNA Clean & Concentrator Kit-100 (Zymo Research, Orange, CA), concentrated using DNA Clean & Concentrator Kit-5 (Zymo Research), and eluted in 10 μL of TE Buffer (10 mmol/L Tris, 0.1 mmol/L EDTA, pH 8.0). Eluted cDNA was denatured at 95°C for 2 minutes and immediately placed on ice for 2 minutes. cDNA was preamplified using the Accel-NGS 1S Plus DNA Library Kit (Swift Biosciences, Ann Arbor, MI). Ten microliters of Adaptase reaction mix containing 3.25 μL of TE Buffer, 2 μL of Buffer G1, 2 μL of Reagent G2, 1.25 μL of Reagent G3, 0.5 μL of Enzyme G4, 0.5 μL of Enzyme G5, and 0.5 μL of Enzyme G6 was added, and the mixture was incubated at 37°C for 15 minutes and at 95°C for 2 minutes. Then 23.5 μL of Extension reaction mix containing 9.25 μL of TE Buffer, 1 μL of Reagent Y1, 3.5 μL of Reagent W2, 8.75 μL of Buffer W3, and 1 μL of Enzyme W4 was added, and the mixture was incubated at 98°C for 30 seconds, at 63°C for 15 seconds, and at 68°C for 5 minutes. Amplified cDNA was then purified using 26.1 μL of AMPure XP beads (Beckman Coulter Diagnostics, Brea, CA) and eluted in 19.5 μL of Buffer EB (Qiagen). To amplify cDNA libraries, each well was mixed with 3 μL of 10 μmol/L i5 primer (5'AATGA-TACGGCGACCACCGAGATCTACAC[i5]ACACTCTTTCCCTACAC GACGCTCTTCCGATCT-3'; IDT), 2.5 μL of 12 μmol/L D7 primer (CAAGCAGAAGACGGCATACGAGATCGAGTAATGTGA CTGGAGTTCAGACGTGTGCTCTTCCGATC-3'; IDT), and 25 μmol/L KAPA HiFi HotStart ReadyMix (KAPA Biosystems, Boston, MA). Amplification was carried out using the following program: 98°C for 3 minutes, 16 cycles of 98°C for 20 seconds, 67°C for 15 seconds, and 72°C for 2 minutes, and a final hold at 72°C for 5 minutes. Each well was then purified using 30 μL of AMPure XP beads, eluted
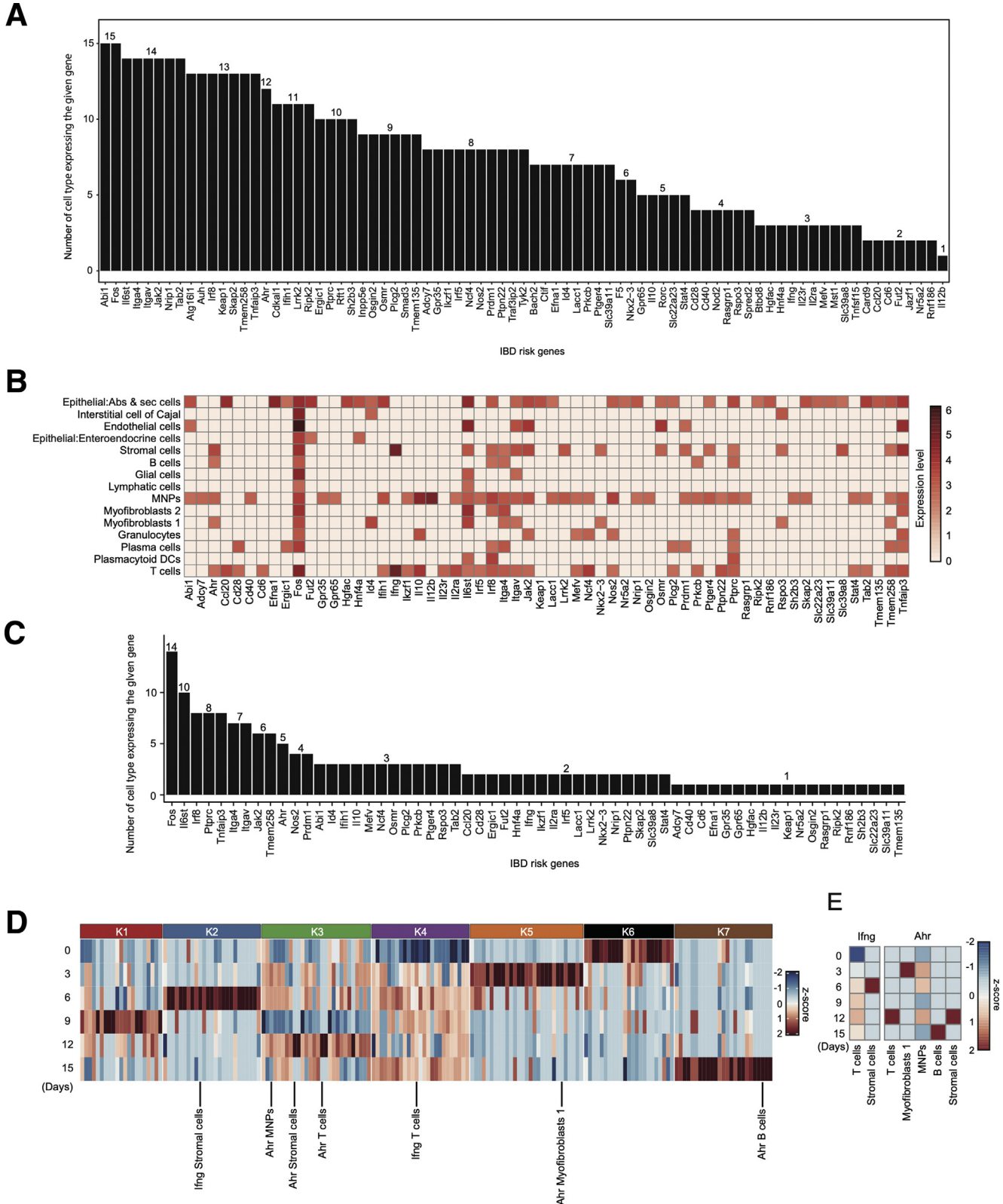
Figure 4. IBD risk genes expressed in multiple cell clusters. (*A*) 79 IBD-related genes that are expressed at one or more time points in at least one of the cell types. (*B*) Heatmap representing expression levels of IBD risk genes. Maximum gene expression levels across time points are shown. (*C*) Number of cell types expressing the given gene. (*D*) Heatmap based on K-means clustering showing expression patterns of IBD risk genes. (*E*) Expression pattern of *Ifng* and *Ahr* across the time course of inflammation.
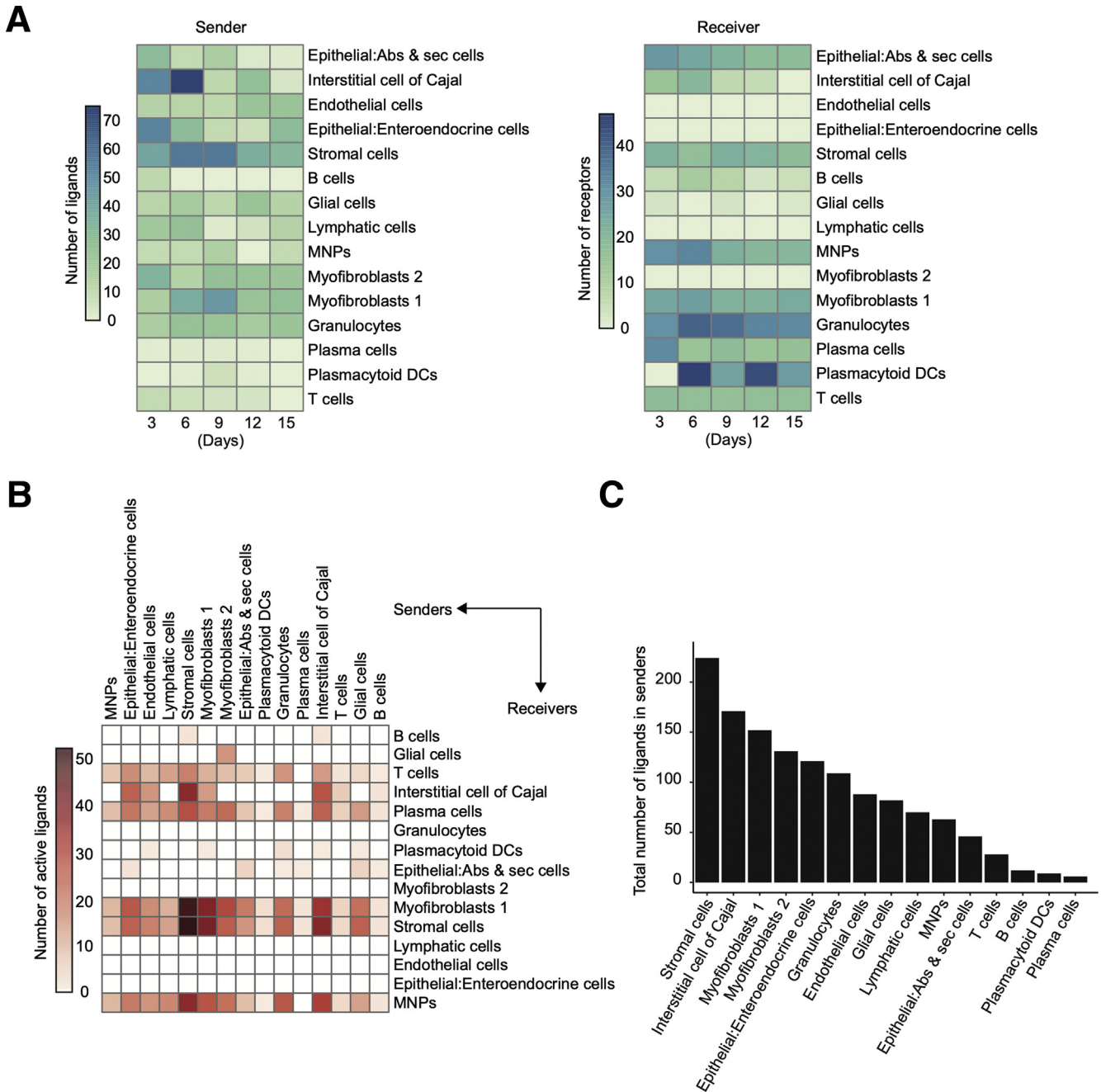
Figure 5. Hub function of stromal cells during inflammation. (*A*) Heatmap showing the number of ligands in senders and receptors in receivers across time points. *Right*: cell type; *bottom*: time point. Analysis conducted using NicheNet.[25] (*B*) Heatmap showing the number of ligand-receptor connections between cells. (*C*) Total number of ligands in senders.

in 30 μL of Buffer EB, and transferred to a new PCR tube. Each well was then again purified using 18 μL of AMPure XP beads and eluted in 10 μL of Buffer EB. In total, 600 pg of amplified cDNA was mixed with water in a total volume of 5 μL. Each well was mixed with 10 μL of Nextera TD buffer (Illumina, San Diego, CA) and 5 μL of Amplicon Tagment enzyme (Illumina) and then incubated at 55°C for 5 minutes to carry out tagmentation. After tagmentation, samples were mixed and purified using AMPure XP beads and eluted in 16 μL of Buffer EB. Eluted DNA was mixed with 2 μL of 10 μmol/L i5 primer, 2 μL of 10 μmol/L P7

primer (5'-CAAGCAGAAGACGGCATACGAGAT[i7]GTCTCGT GGGCTCGG-3'), and 20 μmol/L NEBNext High-Fidelity 2× PCR Master Mix (New England BioLabs). Amplification was carried out using the following program: 72°C for 3 minutes, 98°C for 30 seconds, 8–10 cycles of 98°C for 10 seconds, 66°C for 30 seconds, and 72°C for 1 minute, and a final hold at 72°C for 5 minutes. PCR cycles were determined by qPCR to avoid overamplification. The sequencing libraries were sequenced on the NextSeq500 platform. The read length was set to 20 (read 1) + 8 (i7) + 8 (i5) + 51 (read 2) bases.
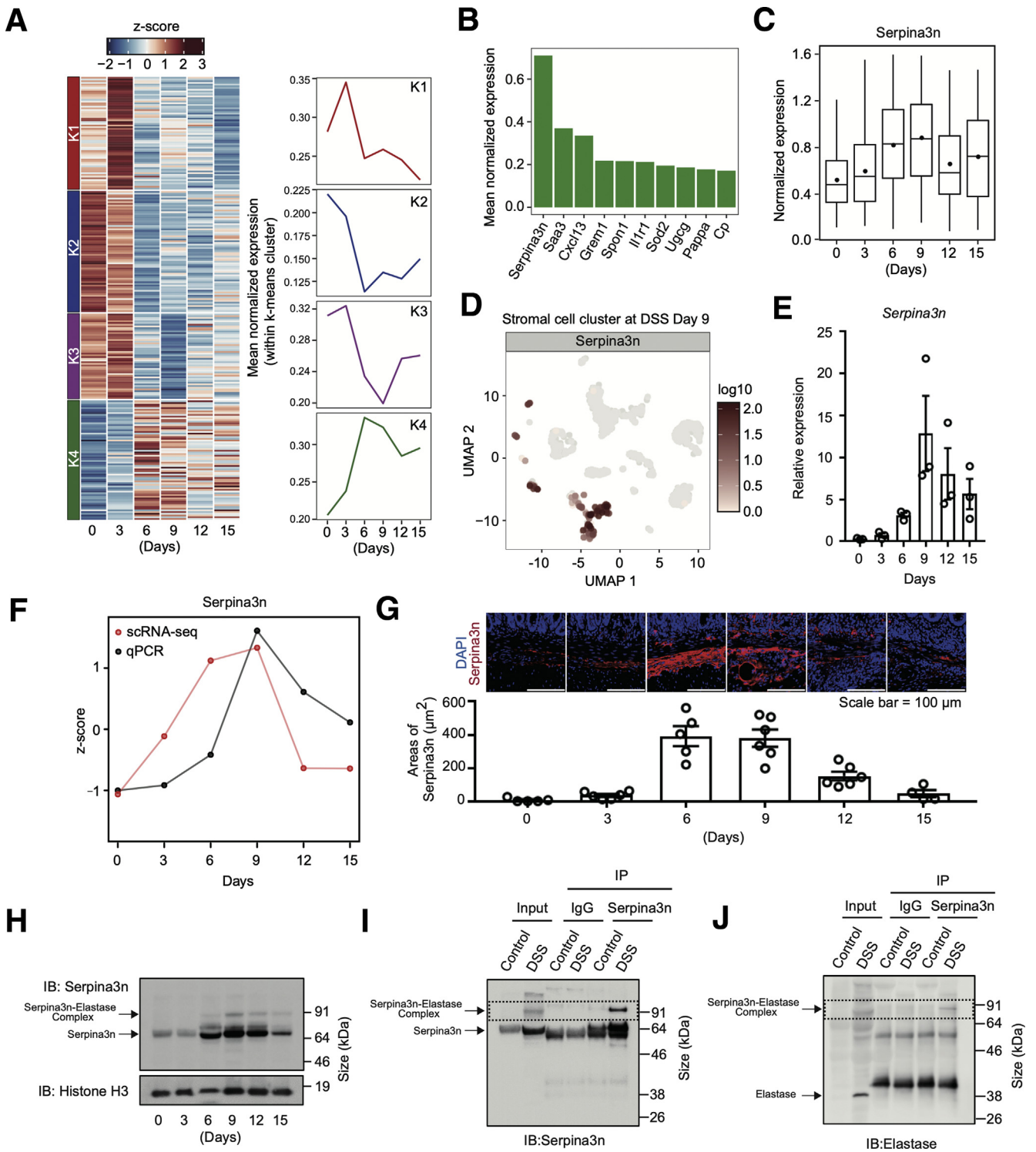
Figure 6. Cell-cell communication during DSS-induced inflammation. Circos plots showing the ligand-receptor links between each cell cluster. *Blunt end of the ribbon* represents the ligand in senders, and *arrowhead* points to the receptor in receivers. The ligand-receptor number is indicated by the size and color of the ribbon.

Immunoprecipitation and Immunoblotting

Tissue lysates were harvested in 1× RIPA buffer: 50 mmol/L Tris-HCl buffer (pH 7.6), 150 mmol/L NaCl, 1% Nonidet P40 Substitute, 0.5% sodium deoxycholate, protease inhibitor cocktail, and 0.1% sodium dodecyl sulfate (Nacalai Tesque). For immunoprecipitation, protein lysates were incubated with primary antibody and Dynabeads protein G (Invitrogen, Carlsbad, CA) according to the manufacturer's protocol. The lysates were boiled and resolved by sodium dodecyl sulfate-polyacrylamide gel electrophoresis and then blotted onto polyvinylidene

Figure 7. Expression and function of Serpina3n in stromal cells during inflammation. (*A*) Heatmap showing the expression patterns of DEGs (across time points) in stromal cells. (*B*) Expression level of genes in the K4 cluster. (*C*) Expression levels of *Serpina3n* across time points. (*D*) UMAP plot showing expression of Serpina3n in the stromal cell cluster (C5) at day 9 in the DSS-induced colitis model. (*E*) mRNA expression of *Serpina3n* in colon was analyzed by real-time qPCR; quantitative result is normalized with *actb*. *P* values were calculated with one-way ANOVA (n = 3 mice for each time point). *P < .001. (*F*) qPCR/scRNA-seq trend comparison was shown in line plot. (*G*) Immunostaining of Serpina3n in the colon of DSS-induced inflammation across the time course. Expression levels were quantified using IMARIS software (BitPlane). Scale bar: 100 μm. *P* values were calculated with one-way ANOVA (n = 3 mice for each time point). *P < .01. (*H*) Western blot of Serpina3n in colon. Histone H3 is an internal control. Bottom: time point. (*I* and *J*) Immunoprecipitation of Serpina3n and blotting with Serpina3n (*F*) or elastase (*G*). Input: whole cell lysate.
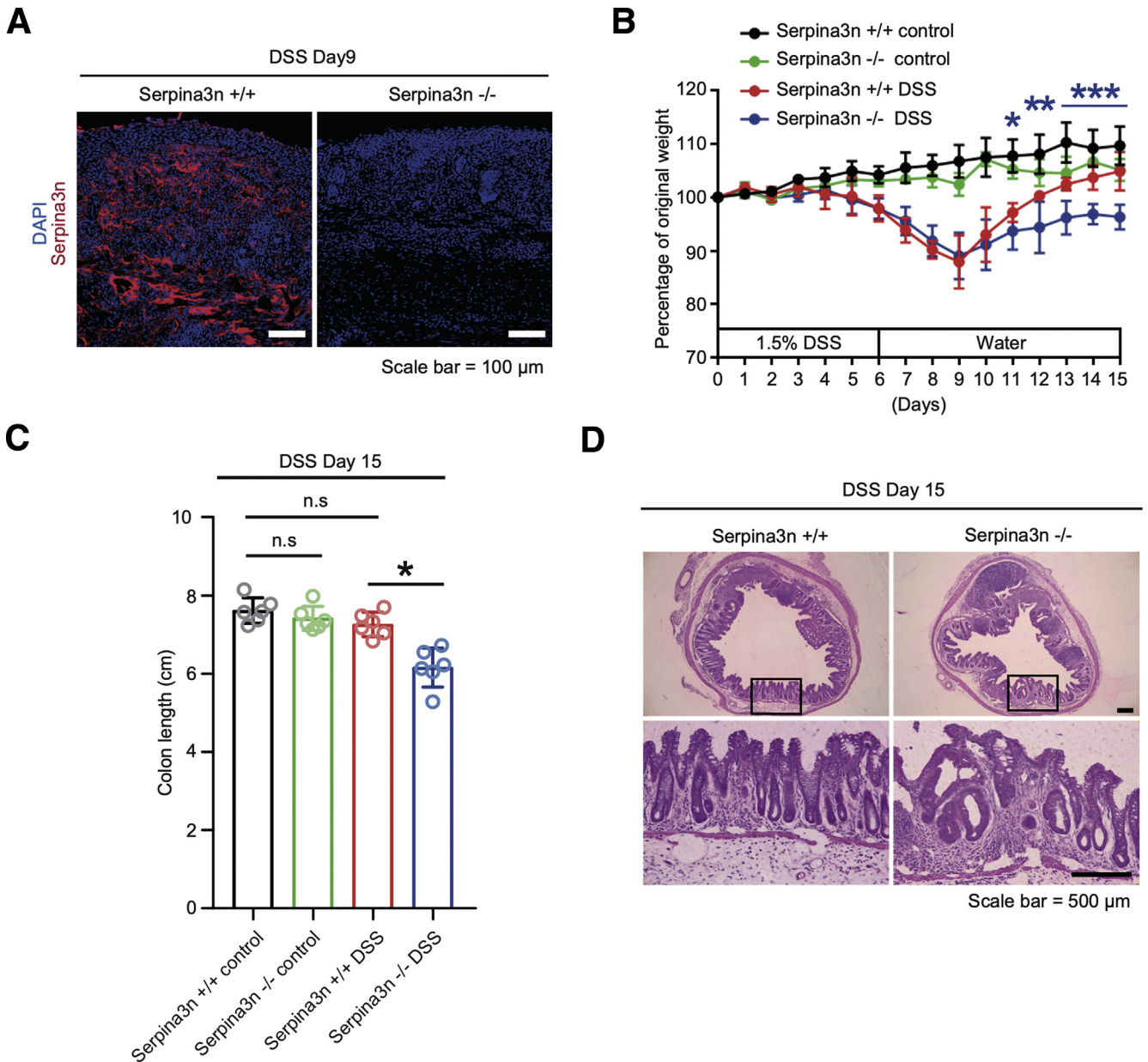
A

DSS Day9

Serpina3n +/+   Serpina3n -/-

DAPI Serpina3n

Scale bar = 100 μm

B

- Serpina3n +/+ control
- Serpina3n -/- control
- Serpina3n +/+ DSS
- Serpina3n -/- DSS

Percentage of original weight

1.5% DSS   Water

(Days)

C

DSS Day 15

Colon length (cm)

Serpina3n +/+ control
Serpina3n -/- control
Serpina3n +/+ DSS
Serpina3n -/- DSS

D

DSS Day 15

Serpina3n +/+   Serpina3n -/-

Scale bar = 500 μm

Figure 8. Serpina3n is involved in the resolution of colon inflammation. (*A*) Expression of *Serpina3n* in the colon was confirmed using immunostaining. Colon samples were collected from wild-type (*Serpina3n* +/+) or *Serpina3n* knockout (*Serpina3n* -/-) mice at day 9 after DSS induction. (*B*) Body weight changes in wild-type (Serpina3n +/+) or Serpina3n knockout (Serpina3n -/-). *P* values were calculated with two-way ANOVA (n = 6 mice per group from 2 independent experiment). *$P <$ .05, **$P <$ .01, ***$P <$ .001. Mean ± standard error of the mean is indicated. (*C*) Colonic length was measured at day 15. *P* values were calculated using one-way ANOVA (n = 6 mice per group from 2 independent experiments). *$P <$ .05. (*D*) Histologic assessment of colon samples (day 15); representative sections were stained with H&E; lower image is a magnified region from the upper image. Scale bar: 500 μm.

difluoride membrane. For Western blot analysis, we used goat polyclonal anti-mouse Serpina3n antibody (R&D Systems), rabbit polyclonal anti-mouse elastase antibody (Abcam, Cambridge, UK), and rabbit polyclonal anti-mouse histone H3 antibody (Abcam). All detected bands were visualized by Chemi-Lumi one L (Nacalai Tesque) and quantified with ImageQuant LAS 4000mini (GE Healthcare, Chicago, IL).

Histochemistry and Immunostaining

Colons were collected at the indicated time points and fixed with 4% paraformaldehyde. Tissue was further incubated with 30% sucrose solution (in PBS) overnight and then embedded in OCT. Cryosections (6-μm thickness) were cut on Cryofilm (Section-lab, Hiroshima, Japan) and blocked with 1% bovine serum albumin in PBS. For the IBD time course, sections were incubated with goat polyclonal

anti-mouse SerpinA3N antibody (1:200; R&D Systems, cat. no. AF4709), rat monoclonal anti-mouse CD19 antibody (1:100; eBioscience, San Diego, CA, cat.no. 14-0193-85),

and goat polyclonal anti mouse S100A8 antibody (1:200; R&D Systems, cat. no. AF3059) at 4°C overnight. The next day, sections were rinsed in PBS and incubated with Alexa
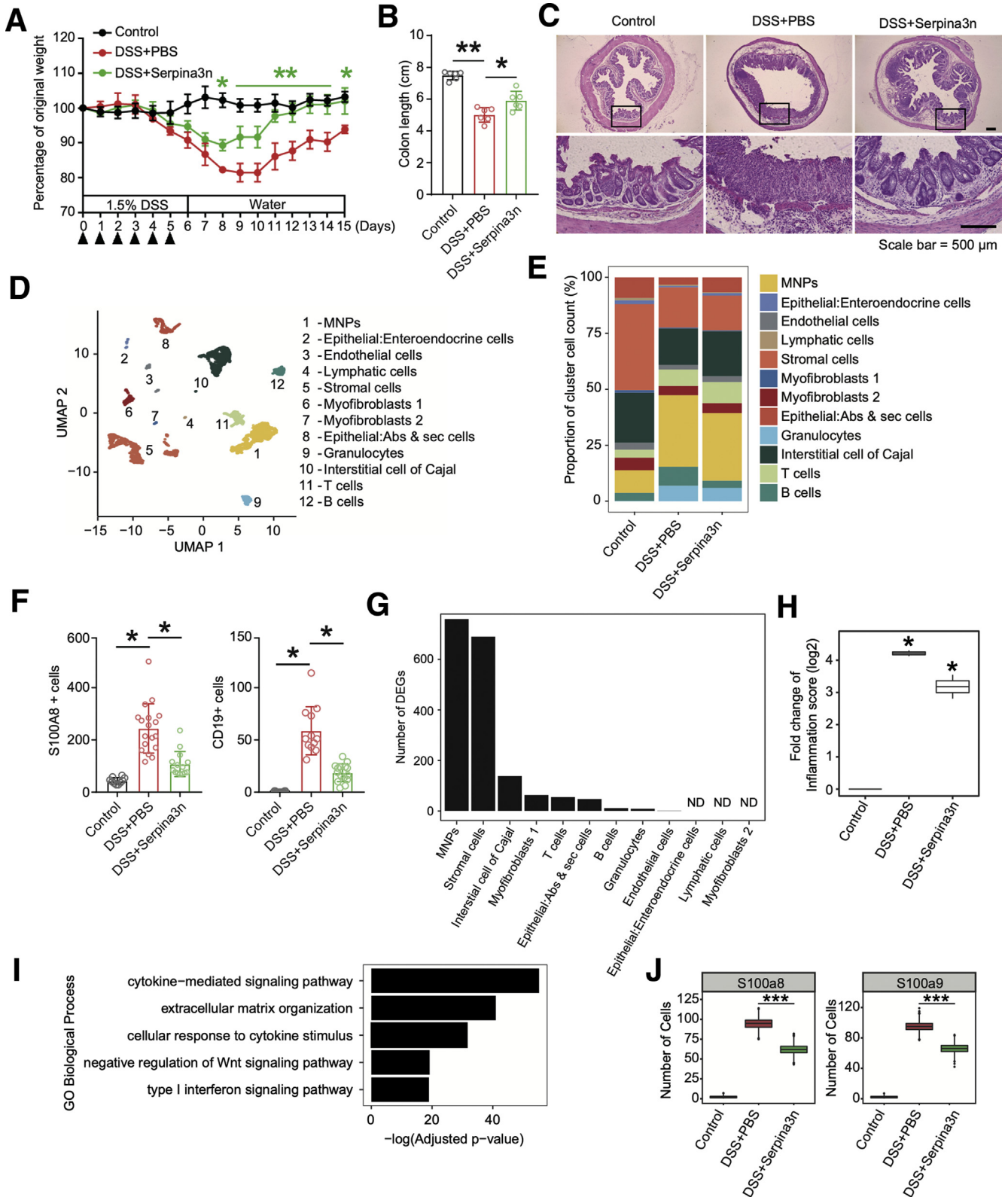
Fluor 488 or Cy3-conjugated secondary antibody (1:200) at room temperature for 1 hour. Nuclei were labeled with DAPI (1:500), and sections were mounted in ProLong Gold antifade mountant (Invitrogen). Images were obtained using confocal microscopy (model A1/C1; Nikon, Tokyo, Japan) using NIS-Elements AR 3.1 software, and images were quantified with IMARIS (Bitplane, Zurich, Switzerland).

Real-Time qPCR

Total RNA from the mouse colon was isolated using Isogene (Nippon) and further purified using the RNeasy Plus Mini kit (Qiagen) according to the manufacturer's instruction. RNA concentration was quantified using the Qubit 3.0 Fluorometer (Thermo Fisher Scientific). cDNA was prepared by reverse transcription using iScript reverse transcription supermix (Bio-Rad, Hercules, CA). Real-time PCR was performed with Thunderbird SYBR qPCR mix (Toyobo, Osaka, Japan), and the following primer sets were used: *Serpina3n*, (forward) 5'-CCCTGAGGAGTGGAAGAAT-3'; (reverse) 5'-CCTGATGCC-CAGCTTTGAAA-3'; *actb*, (forward) 5'-CTAAGGC CAACCGTGAAAAG-3'; (reverse) 5'-ACCAGAGGCATACAG GGACA-3'. Quantitative results were obtained in triplicate, on the basis of the standard curve method, using CFX manager software (Bio-Rad). All data were normalized to *actb*.

Bioinformatics

Preprocessing: from FASTQ to gene expression table. The FASTQ reads were demultiplexed using *bcl2fastq* v2.17.1.14. The barcoded sequence was corrected using an edit distance of less than 2. The corrected reads were then processed using Drop-seq_tools-1.12 (https://github.com/broadinstitute/Drop-seq).[36] The alignment was built using STAR (v2.5b).[37] The mouse reference genome (mm10) was obtained from ftp://ftp.ncbi.nlm.nih.gov/geo/series/GSE63nnn/GSE63472/suppl/GSE63472_mm10_reference_metadata.tar.gz.

Low-quality cells given by the Drop-seq_tool/DigitalExpression output were removed using the number of transcripts, genes, and the percentage of mitochondrial genes for each cell. We set the cutoff empirically. Cells with

the number of total transcripts were higher than at most 150,000 (for time course data), and 50,000 (for *Serpina3n* treated data) were removed. In addition, cells with less than 362 apparently expressed genes (for time course data) and less than 320 apparently expressed genes (for *Serpina3n* treated data) were removed. Last, cells with the percentage of mitochondrial genes higher than 16% were discarded as well. *Downstream analysis overview.* After obtaining gene expression profiles, we followed the common procedure described in the previous study[38] using Monocle3 (https://cole-trapnell-lab.github.io/monocle3/). The Monocle3 workflow includes the following steps: gene expression normalization, cell clustering, UMAP visualization, marker gene identification, pseudotime analysis, and differential gene expression analysis.

Cell Clustering

We used UMAP as a method for dimensionality reduction to define cell clusters.[39] We initially ran UMAP using an *n_neighbors* parameter ranging from 2 to 30. The other parameters were set to default. We visually inspected the clustering structures and set the value to give the lowest number of clusters but to still derive distinguishable cell types, as defined by specific gene markers. We set the *n_neighbors* parameters to 8 and 9 for IBD colon and Serpin treated cell data, respectively. This resulted in identification of 15 clusters in the datasets above. For every cell cluster we listed the top 3 marker genes. They are ranked according to their Monocle3 marker score. Together with cell-type gene signatures curated from published work, we determined the cell type that each cluster represents. Cell proportions were calculated on the basis of the cell count for each cell type normalized by the total cell count at each time point or under each treatment.

Pseudotime and cell trajectory. The pseudotime and cell trajectory analysis is part of the Monocle3 workflow. We selected cells in each cluster using marker genes with the highest specificity score as the starting point of the trajectory.

IBD Risk Gene Analysis

We compiled 96 IBD risk genes from previous studies for analysis.[15–17,19–24] These genes were defined as highly

Figure 9. (*See previous page*). **Serpina3n treatment ameliorates IBD symptoms.** (A) Body weight changes relative to control (*black circle*). DSS-induced mice were intravenously treated with PBS (*red circle*) or Serpina3n (*green circle*). P values were calculated using two-way ANOVA (n = 6 mice per group from 2 independent experiments). $*P < .05$, $**P < .01$, $***P < .001$. (B and C) Colonic length was measured at day 9 of DSS-induced colitis model. P values were calculated using one-way ANOVA (n = 6 mice per group from 2 independent experiments). $*P < .05$, $**P < .01$ (B). Histologic appearance of colon samples (day 9); the lower image is a magnified region of the upper image. Scale bar: 500 μm (C). (D and E) UMAP plot showing the cell clusters in all treatment groups (D). Shown is the proportion of cells (left y-axis) for each cell subset (right y-axis); treatment group is shown on the x-axis (E). (F) Quantification of S100A8-expressing granulocytes and CD19-expressing B cells in control-treated colons (*black bar*), DSS-induced mice treated with PBS (*red bar*) or Serpina3n (*green bar*). P values were calculated using one-way ANOVA. $*P < .01$. (G) Number of DEGs in each cell cluster is shown in the bar graph. ND, no detection of DEGs. (H) Inflammation score was calculated on the basis of inflammatory genes expressed in the MNP cluster. P values were calculated using a one-way ANOVA Bonferroni post-test. $**P < .001$. (I) Gene ontology analysis shows biological pathways enriched in the stromal cell cluster. Bottom: P value. (J) Cell count analysis showing the S100a8 and S100a9 expressing cells within granulocyte cluster in all treatment groups. P values were calculated by one-way ANOVA Bonferroni post-test. $***P < 2e^{-16}$.
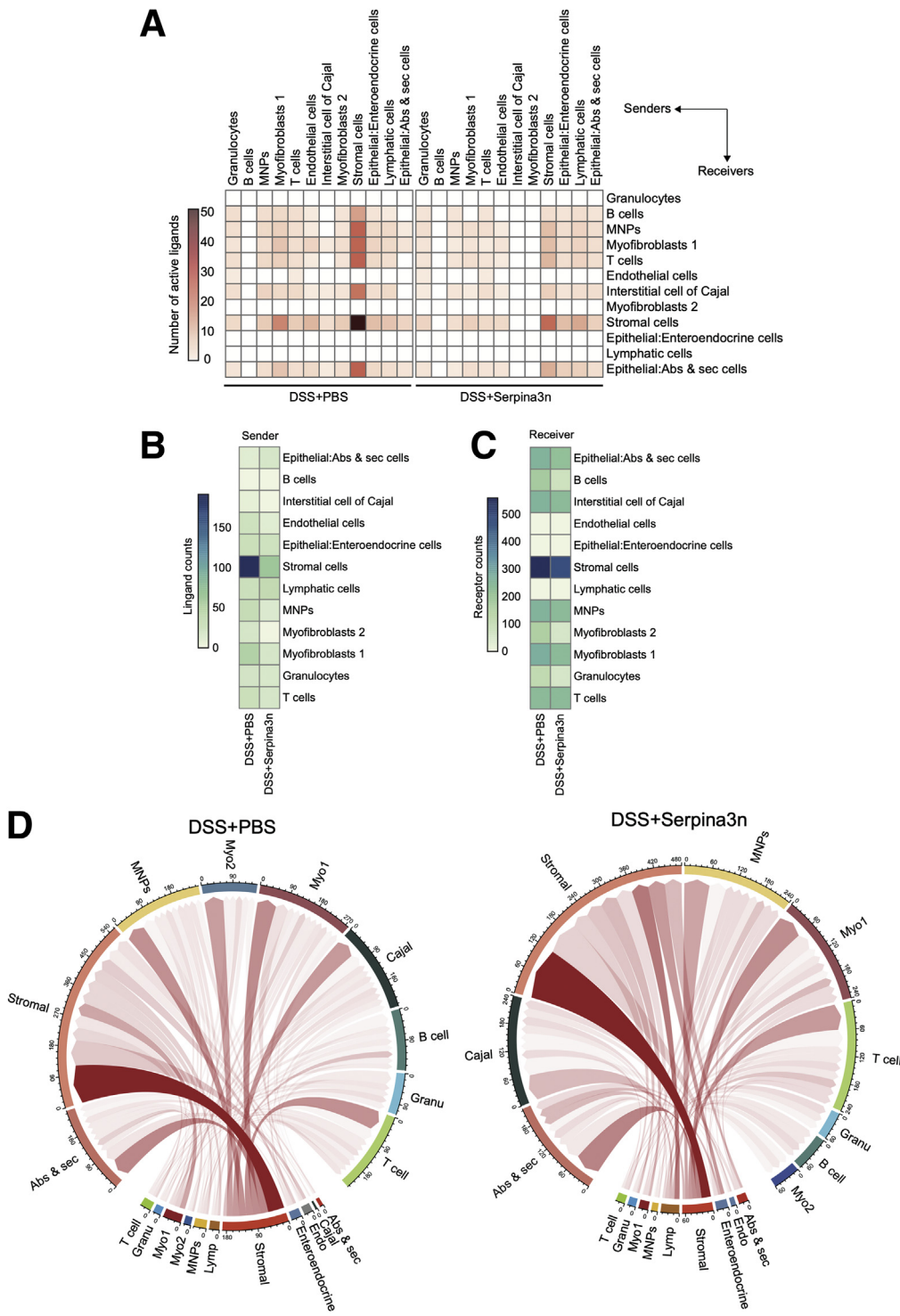
Figure 10. Administration of Serpina3n suppresses cell-cell communication in colitis. (*A*) NicheNet plot showing the ligand-receptor link between the sender and receiver for DSS-induced mice treated with PBS (*left*) or Serpina3n (*right*). (*B* and *C*) Heatmap showing the number of ligands and receptors in cell clusters under DSS-induced group treated with PBS or Serpina3n. (*D*) Circos plot showing ligand-receptor links between clusters in the DSS-induced group treated with PBS or Serpina3n.

expressed if the digital expression level is greater than 5. On the basis of this threshold, we then quantified expression for each cell type and time course point. We also determined the cell types in which each IBD risk gene is expressed.

Differentially Expressed Genes and K-Means Clustering

The DEGs were determined using the Monocle3 regression-based method. In our IBD datasets they were based on the time course, and in Serpin data

they were based on treatment category. In the stromal cell cluster (cluster 5), we further clustered these DEGs on the basis of their gene expression using K-means clustering. To determine the optimal number of clusters, we tried K ranging from 1 to 10 and calculated the sum-of-square metrics. The final K parameter is determined at the point where the metrics drastically change (elbow method). On the basis of our K-means cluster analyses, we identified a set of genes with distinct expression pattern with regard to the actual IBD time course. The trend-plots were calculated by taking the average gene expression at each time point in each K-means cluster.

Quantifying Inflammatory Responses in Macrophages

In our analysis, we quantified the inflammatory response on the basis of M1 inflammatory genes,[40] emphasizing macrophage data in both our IBD and Serpin data. The subset of genes used was obtained from the DEGs, as defined by Monocle3.

The inflammatory response score for the gene set G in a cell type at sample j is calculated as:

$$IR_j = \frac{1}{|M_j|} \cdot \sum_{k \in M_j} \sum_{i \in G} x_{ik} + |M_j|$$

where x_{ik} is the expression level of inflammatory gene i in cell k, Mj is the set of all macrophages, and $|Mj|$ is the total number of cells in sample j. Finally, the amplitude of the inflammatory response is measured in terms of fold change:

$$FC = \frac{IR_j}{IR_0}$$

where $IR0$ is simply the score at the control or non-treated sample.

Analysis of Cell-Cell Interactions Using Ligand Activity

To examine the cell-cell interaction changes over a time course and during Serpin treatment, we used NicheNet[25] ligand activity analysis. NicheNet takes lists of sender cells, receiver cells, and the gene set of interest as its input. We considered all pairwise cell interactions including self-interactions. The cells were further filtered on the basis of the number of expressed genes. In this case, we only selected cells where at least 15% of genes are expressed. The genes of interest were determined on the basis of DEGs of the receiver cell given by Monocle3. We applied this procedure for every sample (ie, time points in IBD data and treatments in our Serpin experiment data). At the end of the procedure we obtained a list of ligands and their activity scores, denoted as a Pearson correlation, for every sender and receiver pair. We finally counted the number of active ligands in every sample after excluding ligands that have appeared in control or non-treated samples.

Functional Analysis

The functional roles of expressed genes in our dataset were determined using gene ontology analysis. For this analysis we used an R-package, Enrichr.[41] The enrichment state was determined using a P value defined by the terms related to biological process. We focused specifically on the terms *inflammatory*, *immunology*, and *wound healing*.

qPCR/scRNA-seq Trend Comparison Analysis

For each time point group, Serpina3n expression from all cells was summed in scRNA-seq data. *Serpina3n* expression of qPCR and scRNA-seq were normalized by *actb*. The expression levels in both analyses were adjusted and plotted by z-score.

References

1. Greten FR, Grivennikov SI. Inflammation and cancer: triggers, mechanisms, and consequences. Immunity 2019;51:27–41.
2. Uderhardt S, Martins AJ, Tsang JS, Lammermann T, Germain RN. Resident macrophages cloak tissue microlesions to prevent neutrophil-driven inflammatory damage. Cell 2019;177:541–555.e17.
3. de Souza HSP, Fiocchi C, Iliopoulos D. The IBD interactome: an integrated view of aetiology, pathogenesis and therapy. Nat Rev Gastroenterol Hepatol 2017;14:739–749.
4. Vilela EG, Torres HO, Martins FP, Ferrari Mde L, Andrade MM, Cunha AS. Evaluation of inflammatory activity in Crohn's disease and ulcerative colitis. World J Gastroenterol 2012;18:872–881.
5. Henderson P, van Limbergen JE, Schwarze J, Wilson DC. Function of the intestinal epithelium and its dysregulation in inflammatory bowel disease. Inflamm Bowel Dis 2011;17:382–395.
6. de Souza HS, Fiocchi C. Immunopathogenesis of IBD: current state of the art. Nat Rev Gastroenterol Hepatol 2016;13:13–27.
7. Gisbert JP, Marin AC, McNicholl AG, Chaparro M. Systematic review with meta-analysis: the efficacy of a second anti-TNF in patients with inflammatory bowel disease whose previous anti-TNF treatment has failed. Aliment Pharmacol Ther 2015;41:613–623.
8. Levin AD, Wildenberg ME, van den Brink GR. Mechanism of action of anti-TNF therapy in inflammatory bowel disease. J Crohns Colitis 2016;10:989–997.
9. Okumura R, Kurakawa T, Nakano T, Kayama H, Kinoshita M, Motooka D, Gotoh K, Kimura T, Kamiyama N, Kusu T, Ueda Y, Wu H, Iijima H, Barman S, Osawa H, Matsuno H, Nishimura J, Ohba Y, Nakamura S, Iida T, Yamamoto M, Umemoto E, Sano K, Takeda K. Lypd8 promotes the segregation of flagellated microbiota and colonic epithelia. Nature 2016;532:117–121.

10. Wirtz S, Popp V, Kindermann M, Gerlach K, Weigmann B, Fichtner-Feigl S, Neurath MF. Chemically induced mouse models of acute and chronic intestinal inflammation. Nature Protocols 2017;12:1295–1309.

11. Picelli S, Bjorklund AK, Faridani OR, Sagasser S, Winberg G, Sandberg R. Smart-seq2 for sensitive full-length transcriptome profiling in single cells. Nat Methods 2013;10:1096–1098.

12. Aran D, Looney AP, Liu L, Wu E, Fong V, Hsu A, Chak S, Naikawadi RP, Wolters PJ, Abate AR, Butte AJ, Bhattacharya M. Reference-based analysis of lung single-cell sequencing reveals a transitional profibrotic macrophage. Nat Immunol 2019;20:163-172.

13. Kinchen J, Chen HH, Parikh K, Antanaviciute A, Jagielowicz M, Fawkner-Corbett D, Ashley N, Cubitt L, Mellado-Gomez E, Attar M, Sharma E, Wills Q, Bowden R, Richter FC, Ahern D, Puri KD, Henault J, Gervais F, Koohy H, Simmons A. Structural remodeling of the human colonic mesenchyme in inflammatory bowel disease. Cell 2018;175:372–386.e17.

14. Parikh K, Antanaviciute A, Fawkner-Corbett D, Jagielowicz M, Aulicino A, Lagerholm C, Davis S, Kinchen J, Chen HH, Alham NK, Ashley N, Johnson E, Hublitz P, Bao L, Lukomska J, Andev RS, Bjorklund E, Kessler BM, Fischer R, Goldin R, Koohy H, Simmons A. Colonic epithelial cell diversity in health and inflammatory bowel disease. Nature 2019;567:49–55.

15. Smillie CS, Biton M, Ordovas-Montanes J, Sullivan KM, Burgin G, Graham DB, Herbst RH, Rogel N, Slyper M, Waldman J, Sud M, Andrews E, Velonias G, Haber AL, Jagadeesh K, Vickovic S, Yao J, Stevens C, Dionne D, Nguyen LT, Villani AC, Hofree M, Creasey EA, Huang H, Rozenblatt-Rosen O, Garber JJ, Khalili H, Desch AN, Daly MJ, Ananthakrishnan AN, Shalek AK, Xavier RJ, Regev A. Intra- and inter-cellular rewiring of the human colon during ulcerative colitis. Cell 2019;178:714–730. e22.

16. Martin JC, Chang C, Boschetti G, Ungaro R, Giri M, Grout JA, Gettler K, Chuang LS, Nayar S, Greenstein AJ, Dubinsky M, Walker L, Leader A, Fine JS, Whitehurst CE, Mbow ML, Kugathasan S, Denson LA, Hyams JS, Friedman JR, Desai PT, Ko HM, Laface I, Akturk G, Schadt EE, Salmon H, Gnjatic S, Rahman AH, Merad M, Cho JH, Kenigsberg E. Single-cell analysis of Crohn's disease lesions identifies a pathogenic cellular module associated with resistance to anti-TNF therapy. Cell 2019;178:1493–1508.e20.

17. Huang B, Chen Z, Geng L, Wang J, Liang H, Cao Y, Chen H, Huang W, Su M, Wang H, Xu Y, Liu Y, Lu B, Xian H, Li H, Li H, Ren L, Xie J, Ye L, Wang H, Zhao J, Chen P, Zhang L, Zhao S, Zhang T, Xu B, Che D, Si W, Gu X, Zeng L, Wang Y, Li D, Zhan Y, Delfouneso D, Lew AM, Cui J, Tang WH, Zhang Y, Gong S, Bai F, Yang M, Zhang Y. Mucosal profiling of pediatric-onset colitis and IBD reveals common pathogenics and therapeutic pathways. Cell 2019; 179:1160–1176.e24.

18. Wang Y, Song W, Wang J, Wang T, Xiong X, Qi Z, Fu W, Yang X, Chen YG. Single-cell transcriptome analysis reveals differential nutrient absorption functions in human intestine. J Exp Med 2020;217.

19. Jostins L, Ripke S, Weersma RK, Duerr RH, McGovern DP, Hui KY, Lee JC, Schumm LP, Sharma Y, Anderson CA, Essers J, Mitrovic M, Ning K, Cleynen I, Theatre E, Spain SL, Raychaudhuri S, Goyette P, Wei Z, Abraham C, Achkar JP, Ahmad T, Amininejad L, Ananthakrishnan AN, Andersen V, Andrews JM, Baidoo L, Balschun T, Bampton PA, Bitton A, Boucher G, Brand S, Buning C, Cohain A, Cichon S, D'Amato M, De Jong D, Devaney KL, Dubinsky M, Edwards C, Ellinghaus D, Ferguson LR, Franchimont D, Fransen K, Gearry R, Georges M, Gieger C, Glas J, Haritunians T, Hart A, Hawkey C, Hedl M, Hu X, Karlsen TH, Kupcinskas L, Kugathasan S, Latiano A, Laukens D, Lawrance IC, Lees CW, Louis E, Mahy G, Mansfield J, Morgan AR, Mowat C, Newman W, Palmieri O, Ponsioen CY, Potocnik U, Prescott NJ, Regueiro M, Rotter JI, Russell RK, Sanderson JD, Sans M, Satsangi J, Schreiber S, Simms LA, Sventoraityte J, Targan SR, Taylor KD, Tremelling M, Verspaget HW, De Vos M, Wijmenga C, Wilson DC, Winkelmann J, Xavier RJ, Zeissig S, Zhang B, Zhang CK, Zhao H, International IBDGC, Silverberg MS, Annese V, Hakonarson H, Brant SR, Radford-Smith G, Mathew CG, Rioux JD, Schadt EE, Daly MJ, Franke A, Parkes M, Vermeire S, Barrett JC, Cho JH. Host-microbe interactions have shaped the genetic architecture of inflammatory bowel disease. Nature 2012;491:119–124.

20. Liu JZ, van Sommeren S, Huang H, Ng SC, Alberts R, Takahashi A, Ripke S, Lee JC, Jostins L, Shah T, Abedian S, Cheon JH, Cho J, Dayani NE, Franke L, Fuyuno Y, Hart A, Juyal RC, Juyal G, Kim WH, Morris AP, Poustchi H, Newman WG, Midha V, Orchard TR, Vahedi H, Sood A, Sung JY, Malekzadeh R, Westra HJ, Yamazaki K, Yang SK, International Multiple Sclerosis Genetics C, International IBDGC, Barrett JC, Alizadeh BZ, Parkes M, Bk T, Daly MJ, Kubo M, Anderson CA, Weersma RK. Association analyses identify 38 susceptibility loci for inflammatory bowel disease and highlight shared genetic risk across populations. Nat Genet 2015;47:979–986.

21. de Lange KM, Moutsianas L, Lee JC, Lamb CA, Luo Y, Kennedy NA, Jostins L, Rice DL, Gutierrez-Achury J, Ji SG, Heap G, Nimmo ER, Edwards C, Henderson P, Mowat C, Sanderson J, Satsangi J, Simmons A, Wilson DC, Tremelling M, Hart A, Mathew CG, Newman WG, Parkes M, Lees CW, Uhlig H, Hawkey C, Prescott NJ, Ahmad T, Mansfield JC, Anderson CA, Barrett JC. Genome-wide association study implicates immune activation of multiple integrin genes in inflammatory bowel disease. Nat Genet 2017;49:256–261.

22. Huang H, Fang M, Jostins L, Umicevic Mirkov M, Boucher G, Anderson CA, Andersen V, Cleynen I, Cortes A, Crins F, D'Amato M, Deffontaine V, Dmitrieva J, Docampo E, Elansary M, Farh KK, Franke A,

Gori AS, Goyette P, Halfvarson J, Haritunians T, Knight J, Lawrance IC, Lees CW, Louis E, Mariman R, Meuwissen T, Mni M, Momozawa Y, Parkes M, Spain SL, Theatre E, Trynka G, Satsangi J, van Sommeren S, Vermeire S, Xavier RJ, International Inflammatory Bowel Disease Genetics C, Weersma RK, Duerr RH, Mathew CG, Rioux JD, McGovern DPB, Cho JH, Georges M, Daly MJ. , Barrett JC. Fine-mapping inflammatory bowel disease loci to single-variant resolution. Nature 2017;547:173–178.

23. Mohanan V, Nakata T, Desch AN, Levesque C, Boroughs A, Guzman G, Cao Z, Creasey E, Yao J, Boucher G, Charron G, Bhan AK, Schenone M, Carr SA, Reinecker HC, Daly MJ, Rioux JD, Lassen KG, Xavier RJ. C1orf106 is a colitis risk gene that regulates stability of epithelial adherens junctions. Science 2018;359:1161–1166.

24. Graham DB, Xavier RJ. Pathway paradigms revealed from the genetics of inflammatory bowel disease. Nature 2020;578:527–539.

25. Browaeys R, Saelens W, Saeys Y. NicheNet: modeling intercellular communication by linking ligands to target genes. Nat Methods 2020;17:159–162.

26. Winkels H, Ehinger E, Vassallo M, Buscher K, Dinh HQ, Kobiyama K, Hamers AAJ, Cochain C, Vafadarnejad E, Saliba AE, Zernecke A, Pramod AB, Ghosh AK, Anto Michel N, Hoppe N, Hilgendorf I, Zirlik A, Hedrick CC, Ley K, Wolf D. Atlas of the immune cell repertoire in mouse atherosclerosis defined by single-cell RNA-sequencing and mass cytometry. Circ Res 2018;122:1675–1688.

27. Barry R, Ruano-Gallego D, Radhakrishnan ST, Lovell S, Yu L, Kotik O, Glegola-Madejska I, Tate EW, Choudhary JS, Williams HRT, Frankel G. Faecal neutrophil elastase-antiprotease balance reflects colitis severity. Mucosal Immunol 2020;13:322–333.

28. Vicuna L, Strochlic DE, Latremoliere A, Bali KK, Simonetti M, Husainie D, Prokosch S, Riva P, Griffin RS, Njoo C, Gehrig S, Mall MA, Arnold B, Devor M, Woolf CJ, Liberles SD, Costigan M, Kuner R. The serine protease inhibitor SerpinA3N attenuates neuropathic pain by inhibiting T cell-derived leukocyte elastase. Nat Med 2015; 21:518–523.

29. Law RH, Zhang Q, McGowan S, Buckle AM, Silverman GA, Wong W, Rosado CJ, Langendorf CG, Pike RN, Bird PI, Whisstock JC. An overview of the serpin superfamily. Genome Biol 2006;7:216.

30. Foell D, Wittkowski H, Ren Z, Turton J, Pang G, Daebritz J, Ehrchen J, Heidemann J, Borody T, Roth J, Clancy R. Phagocyte-specific S100 proteins are released from affected mucosa and promote immune responses during inflammatory bowel disease. J Pathol 2008; 216:183–192.

31. Voisin MB, Leoni G, Woodfin A, Loumagne L, Patel NS, Di Paola R, Cuzzocrea S, Thiemermann C, Perretti M, Nourshargh S. Neutrophil elastase plays a nonredundant role in remodeling the venular basement membrane and neutrophil diapedesis post-ischemia/ reperfusion injury. J Pathol 2019;248:88–102.

32. Neurath MF. Current and emerging therapeutic targets for IBD. Nat Rev Gastroenterol Hepatol 2017; 14:269–278.

33. Ohtsuka M, Sato M, Miura H, Takabayashi S, Matsuyama M, Koyano T, Arifin N, Nakamura S, Wada K, Gurumurthy CB. i-GONAD: a robust method for in situ germline genome engineering using CRISPR nucleases. Genome Biol 2018;19:25.

34. Labun K, Montague TG, Krause M, Torres Cleuren YN, Tjeldnes H, Valen E. CHOPCHOP v3: expanding the CRISPR web toolbox beyond genome editing. Nucleic Acids Res 2019;47:W171–W174.

35. Whittem CG, Williams AD, Williams CS. Murine colitis modeling using dextran sulfate sodium (DSS). J Vis Exp 2010;35:1652.

36. Macosko EZ, Basu A, Satija R, Nemesh J, Shekhar K, Goldman M, Tirosh I, Bialas AR, Kamitaki N, Martersteck EM, Trombetta JJ, Weitz DA, Sanes JR, Shalek AK, Regev A, McCarroll SA. Highly parallel genome-wide expression profiling of individual cells using nanoliter droplets. Cell 2015;161:1202–1214.

37. Dobin A, Davis CA, Schlesinger F, Drenkow J, Zaleski C, Jha S, Batut P, Chaisson M, Gingeras TR. STAR: ultrafast universal RNA-seq aligner. Bioinformatics 2013; 29:15–21.

38. Cao JY, Spielmann M, Qiu XJ, Huang XF, Ibrahim DM, Hill AJ, Zhang F, Mundlos S, Christiansen L, Steemers FJ, Trapnell C, Shendure J. The single-cell transcriptional landscape of mammalian organogenesis. Nature 2019;566:496–502.

39. Becht E, McInnes L, Healy J, Dutertre CA, Kwok IWH, Ng LG, Ginhoux F, Newell EW. Dimensionality reduction for visualizing single-cell data using UMAP. Nat Biotechnol 2018.

40. Mould KJ, Jackson ND, Henson PM, Seibold M, Janssen WJ. Single cell RNA sequencing identifies unique inflammatory airspace macrophage subsets. JCI Insight 2019;4.

41. Kuleshov MV, Jones MR, Rouillard AD, Fernandez NF, Duan Q, Wang Z, Koplev S, Jenkins SL, Jagodnik KM, Lachmann A, McDermott MG, Monteiro CD, Gundersen GW, Ma'ayan A. Enrichr: a comprehensive gene set enrichment analysis web server 2016 update. Nucleic Acids Res 2016;44:W90–W97.

Correspondence
Address correspondence to: Takashi Shimbo, PhD, or Katsuto Tamai, MD, PhD, Department of Stem Cell Therapy Science, Graduate School of Medicine, Osaka University, Suita, Japan. e-mail: shimbot@sts.med.osaka-u.ac.jp or tamai@gts.med.osaka-u.ac.jp; fax: +81-6-6210-8399.

CRediT Authorship Contributions
    Yen-Ting Ho, PhD (Investigation: Lead; Methodology: Lead; Visualization: Lead; Writing – original draft: Lead)

Takashi Shimbo, PhD (Conceptualization: Lead; Data curation: Lead; Project administration: Lead; Supervision: Lead; Writing – original draft: Lead; Writing – review & editing: Lead)

Edward Wijaya, PhD (Data curation: Equal; Formal analysis: Equal; Visualization: Equal)

Tomomi Kitayama, MS (Investigation: Supporting; Methodology: Supporting; Resources: Supporting)

Satoshi Takaki, MS (Investigation: Supporting; Methodology: Supporting; Resources: Supporting)

Yuya Ouchi, MS (Data curation: Supporting; Formal analysis: Supporting)

Kentaro Ikegami, PhD (Formal analysis: Supporting; Visualization: Supporting)

Kazuya Miyashita, PhD (Formal analysis: Supporting; Visualization: Supporting)

Eiichi Takaki, PhD (Methodology: Supporting; Resources: Supporting)

Ryoma Yamamoto, PhD (Data curation: Supporting; Formal analysis: Supporting)

Yasufumi Kaneda, MD, PhD (Supervision: Lead; Writing – review & editing: Lead)

Katsuto Tamai, MD, PhD (Funding acquisition: Lead; Supervision: Lead; Writing – review & editing: Lead)

Conflicts of interest

Funding